Kovove Mater. 52 2014 345–351
DOI: 10.4149/km_2014_6_345

Dehydriding behaviour of electrochemically hydrided Mg-Ni-Mm alloys

V. Knotek[1]*, M. Lhotka[2], D. Vojtěch[1]

[1] *Department of Metals and Corrosion Engineering, Institute of Chemical Technology Prague, Technická 5, 166 28 Prague 6, Czech Republic*
[2] *Department of Inorganic Technology, Institute of Chemical Technology Prague, Technická 5, 166 28 Prague 6, Czech Republic*

Received 16 January 2014, received in revised form 14 May 2014, accepted 16 May 2014

Abstract

Powder samples of three binary Mg-Ni alloys and one ternary Mg-Ni-Mm alloy were electrochemically hydrided and subjected to the temperature-programmed desorption technique. The powders were prepared by mechanical grinding of appropriate as-cast alloy ingots. The alloy samples were hydrided in a 6 M KOH solution at 80 °C for 240 min and at 20 mA g^{-1}. The structures of the alloys were studied using optical microscopy. The phase compositions of the samples were determined by X-ray diffraction. The formation of MgH_2 and $Mg(OH)_2$ was observed after hydriding in all of the investigated alloys. It was found that the concentration of absorbed hydrogen depends on the eutectic fraction in the structure and on the hydroxide-formation resistance. In contrast, the decomposition temperature of MgH_2 likely depends on the amounts of both alloying elements and magnesium hydroxide. Compared to pure commercial MgH_2, the decomposition temperatures of MgH_2 in the investigated alloys were reduced by more than 200 °C.

K e y w o r d s: magnesium alloys, rare earth, thermally activated processes

1. Introduction

The earliest interest in the hydrogen economy, i.e., the utilisation of hydrogen as a universal energy carrier, can be traced to the oil crisis of the 1970s. Some decades later, the idea of a hydrogen economy is still alive; moreover, the interest in hydrogen has been increasing in recent years. In fact, a hydrogen economy may hold the answers to questions such as climate change and fossil-fuel dependence. However, until safe, simple and cost-efficient methods of hydrogen storage are developed, the hydrogen economy cannot evolve.

Recently, the most widely employed methods of storing hydrogen involve compressed and liquefied hydrogen in appropriate containers. However, the disadvantages of these methods are the low energy density of the stored hydrogen and the high consumption of energy during compression or liquefaction [1]. Since $LaNi_5$- and FeTi-based hydrides were discovered and started to be used at the commercial level [2, 3], the storage of hydrogen in metal hydrides has attracted considerable attention. Especially hydrides based on magnesium, which is able to absorb approximately five times higher amount of hydrogen than $LaNi_5$ [4], are prospective materials to become ideal storage materials. The main advantages of magnesium are its low density, non-toxicity, availability and ability to absorb a large amount of hydrogen (7.6 wt.% in stoichiometric MgH_2). Unfortunately, disadvantages, such as the high thermodynamic stability of MgH_2 and the slow kinetics of magnesium hydrogenation, inhibit the practical usage of magnesium.

Various efforts have been made to destabilise the MgH_2 phase, which would improve its hydriding/dehydriding behaviour. These strategies include i) the addition of transition metals (Ni, Cu, Co, Mn, Zn) and rare earths to form complex hydrides, such as Mg_2NiH_4, Mg_2CoH_5, Mg_3MnH_7, Mg_2RENiH_7, $MgZnH_3$ [5–9]. These complex hydrides usually decompose at lower temperatures than the MgH_2 phase,

*Corresponding author: tel.: +420220444055; fax: +420220444400; e-mail address: Vitezslav.Knotek@vscht.cz

but they achieve lower gravimetric concentrations of hydrogen. Another strategy to enhance the hydriding performance of magnesium is ii) the application of catalysts, e.g., transition metals [10], metal oxides [11, 12], halides [13], or carbon [14]. The last approach consists of iii) the preparation of nanocrystalline or amorphous structures, which are obtained, in most cases, by ball milling or rapid solidification [15–17]. Ball milling during hydriding breaks down the naturally formed hydride layer that decreases the further diffusion of hydrogen. Moreover, both ball milling and rapid solidification lead to a fine structure of Mg with a number of lattice defects, grain boundaries and interfaces, which are beneficial for the thermodynamics and kinetics of the hydriding/dehydriding process [18].

For the preparation of metallic hydrides, we can use either a gas hydriding or an electrochemical hydriding process. Electrochemical hydriding is beneficial because it generates atomic hydrogen, which can easily penetrate the structure and form hydrides. Another benefit is its mild hydriding conditions. Therefore, electrochemical hydriding has been used many times by scientists to test new materials for secondary batteries with high energy capacities [19]. In particular, Mg-based alloys are widely studied in this way [16, 20–22]; the hydrogen capacities of these materials in mAh g^{-1} can be found in the literature. These values can be converted to capacities in units of wt.% hydrogen. However, the true concentrations of hydrogen in electrochemically hydrided Mg-based alloys may be significantly higher because room temperature, at which electrochemical discharging is often performed, is not sufficient to release all the fixed hydrogen in hydrides. For example, a hydrided Mg_2Ni alloy that was prepared via hydriding combustion synthesis (HCS) has demonstrated an approximate capacity of 3.5 wt.% hydrogen [6]. However, the same alloy, when treated under similar conditions (HCS), showed a discharged capacity of only 39 mAh g^{-1}, which corresponds to 0.15 wt.% hydrogen [23]. Nonetheless, to the best of our knowledge, only a few papers have been devoted to the measurement of the true concentrations of hydrogen in electrochemically hydrided alloys [24].

Therefore, in our previous paper, we evaluated the actual surface hydrogen concentrations of bulk Mg-based alloys after electrochemical hydriding [25]. Because nickel and mischmetal are known to positively affect hydrogen absorption, we subjected Mg-Ni-Mm alloys to electrochemical hydriding in this study. Both the amount of absorbed hydrogen and the temperature of hydrogen desorption for hydrided alloys were determined. It will be shown that the achieved hydrogen concentrations approach those of commercial transition-metal-based hydrides and that the hydrogen-evolution temperatures are significantly lower compared to that of pure MgH_2.

Table 1. Chemical compositions of the investigated alloys

Alloy designation	Element (wt.%)					
MgNi15	14.8	–	–	–	–	–
MgNi26	26.4	–	–	–	–	–
MgNi34	34.2	–	–	–	–	–
MgNi26Mm12	25.8	6.0	3.0	2.1	0.6	11.7

2. Experiment

Powders of three binary Mg-Ni alloys and one ternary Mg-Ni-Mm alloy (Mm denotes mischmetal containing 45 % Ce, 38 % La, 12 % Nd, and 4 % Pr), of which the compositional details are given in Table 1, were subjected to electrochemical hydriding. Powders with particles 40–130 μm in size were prepared by the mechanical machining of ingots of the appropriate as-cast alloys. The alloy ingots were prepared by the induction melting of pure Mg, Ni and Mm (99.9 % purity) under a protective atmosphere of argon.

Prior to electrochemical hydriding, the alloy powders were uniaxially cold pressed into pellets at 750 MPa. Each pellet weighed 0.5 g and had a diameter of 16 mm and a length of 2 mm. The pellets were electrochemically hydrided in a 6 M KOH solution at 80 ℃ for 240 min using a galvanostatic method with a current density of 20 mA g^{-1}.

The structures of the as-cast alloys were observed by light microscopy (LM), scanning electron microscopy (SEM, TESCAN Vega 3) and energy-dispersive spectrometry (EDS, OXFORD INSTRUMENT Inca 350). The phase compositions of the alloys both before and after hydriding were determined by X-ray diffraction (XRD, X Pert Pro, Cu Kα radiation).

Both the hydrogen concentrations in the hydrided samples and the temperatures of hydrogen evolution were determined via the temperature-programmed desorption technique (TPD, MICROMETRICS AutoChem II 2920). In addition to the hydrided samples, we also investigated the behaviour of pure MgH_2 powder (20 μm, 98 %, HiChem) under the same conditions. Each sample was pretreated in Ar gas at 273 K before hydrogen desorption. The desorption analysis was carried out in a reactor by heating under programmed temperature control from the ambient temperature to 673 K at a heating rate of 4 K min^{-1} using argon (50 ml min^{-1}). The gas stream leaving the reactor was passed through a water-vapour trap at 210 K, and the evolution of the hydrogen was detected using a thermal conductivity detector. At the end of each experiment, the reactor that contained the examined sample was cooled down to reach the baseline, and calibration of the system was performed.

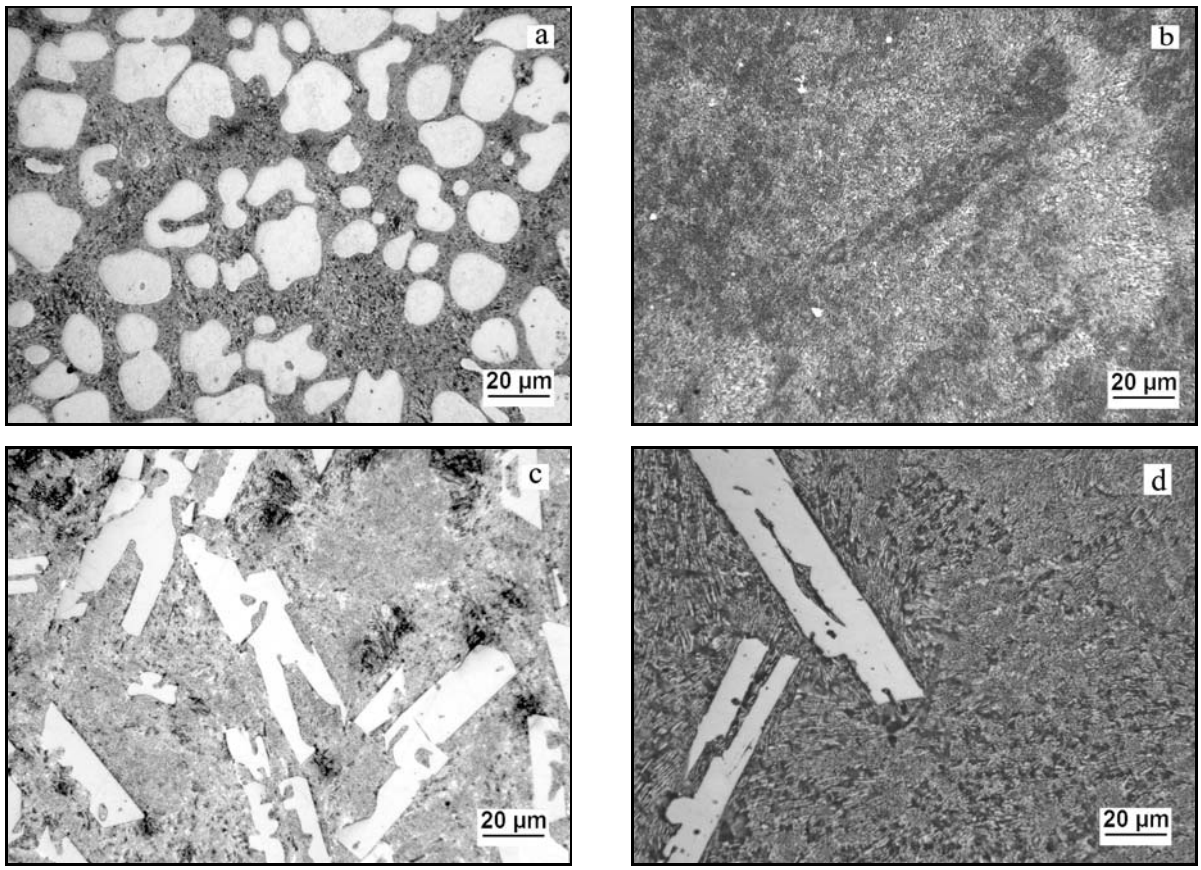

Fig. 1. Microstructures of the investigated alloys (light microscope): (a) MgNi15, (b) MgNi26, (c) MgNi34, (d) MgNi26Mm12.

3. Results and discussion

3.1. Structures of alloys

Light micrographs of the as-cast alloys are presented in Fig. 1. The structures of the binary Mg-Ni alloys (Fig. 1a–c) correspond to those of a typical eutectic system. The MgNi15 alloy is hypoeutectic (Fig. 1a) and consists of α-Mg dendrites (light) and α-Mg + Mg_2Ni eutectic (dark). Because the eutectic point of the Mg-Ni alloys corresponds to 23.5 wt.% Ni, the binary MgNi26 and MgNi34 alloys are hypereutectic. However, the structures of these two hypereutectic alloys (Fig. 1b,c) are very different. While the structure of the MgNi26 alloy (Fig. 1b) is dominated by a very fine α-Mg + Mg_2Ni eutectic mixture and by very small white grains of the primary Mg_2Ni phase, the structure of the MgNi34 alloy (Fig. 1c) is formed by the α-Mg + Mg_2Ni eutectic mixture (dark) and large sharp-edged polyhedral Mg_2Ni crystals (light). The ternary MgNi26Mm12 alloy (Fig. 1d) exhibits a hypereutectic structure. XRD and EDS analyses revealed the presence of the primary Mg_2Ni phase (light) and a ternary α-Mg + Mg_2Ni + $Mg_{12}Mm$ eutectic mixture (dark). As stated in the previous section, Mm denotes a mixture of La, Ce, Nd, and Pr; therefore, the $Mg_{12}Mm$ phase consists of a solid solution of isostructural $Mg_{12}La$ and $Mg_{12}Ce$, $Mg_{12}Nd$, and $Mg_{12}Pr$ (space group I4/mmm) phases [26].

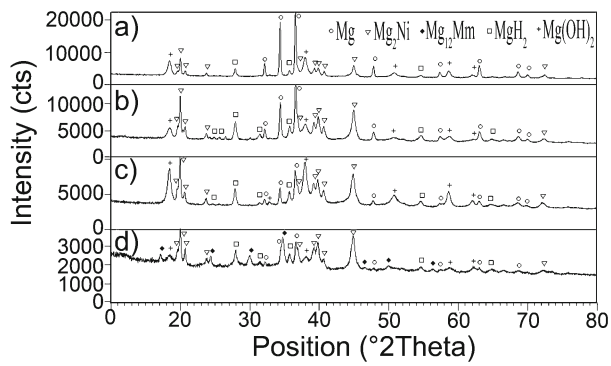

Fig. 2. XRD patterns of the (a) MgNi15, (b) MgNi26, (c) MgNi34 and (d) MgNi26Mm12 alloys after electrochemical hydriding at 80 °C for 240 min.

3.2. Phase composition after hydriding

Figure 2 shows the results of XRD analyses of the hydrided alloys. These results indicate that only two new phases – MgH_2 and $Mg(OH)_2$ – appeared

Table 2. XRD area ratios of $MgH_2/Mg(OH)_2$ for the investigated alloys after hydriding

Alloy	MgNi15	MgNi26	MgNi34	MgNi26Mm12
Area ratio of $MgH_2/Mg(OH)_2$ peaks	0.37	1.12	0.26	0.81

in all of the investigated alloys after electrochemical hydriding. No more complex hydrides, such as Mg_2NiH_4 or mischmetal containing hydride, were detected; however, these hydrides are often mentioned in studies that have utilised gas hydriding at high temperatures and pressures [8, 17, 27]. The difference could be attributed to an insufficient energy input for the phase transformation, as electrochemical hydriding operates under mild conditions. For example, there is a large energy barrier for the transformation of $Mg_2NiH_{0.3}$ (hydrogen solid solution in the Mg_2Ni phase) to Mg_2NiH_4, which is caused by the significant differences in the lattice parameters. The $Mg_2NiH_{0.3}$ phase is characterised by the $P6_222$ space group with lattice parameters $a = 0.524$ nm and $c = 1.333$ nm [28], whereas the low-temperature hydride is of the $C2/c$ space group with parameters $a = 1.434$ nm, $b = 0.640$ nm and $c = 0.648$ nm [29]. Alternatively, the MgH_2 hydride is of the $P42/mnm$ space group with lattice parameters $a = 0.452$ nm and $c = 0.302$ nm [28]. By comparing these parameters to those of α-Mg ($P63/mmc$ space group with parameters $a = 0.324$ nm and $c = 0.526$ nm [28]), it can be assumed that the transformation to MgH_2 (reaction 1) proceeds more readily and quickly than the transformation from the $Mg_2NiH_{0.3}$ phase to the Mg_2NiH_4 hydride [7, 28].

$$Mg + 2H \rightarrow MgH_2. \quad (1)$$

Magnesium hydroxide is present on the surface because it grows as a result of the reaction of magnesium or magnesium hydride with water, according to reactions (2) or (3), respectively:

$$Mg + 2H_2O \rightarrow Mg(OH)_2 + H_2, \quad (2)$$

$$MgH_2 + 2H_2O \rightarrow Mg(OH)_2 + 2H_2. \quad (3)$$

Based on the results of the XRD analyses of the alloys after hydriding, we can determine the differences in volume of the MgH_2 and $Mg(OH)_2$ fractions between the investigated alloys. These differences may serve as a guide to suggest the mechanism of the electrochemical hydriding. For this purpose, we determined the area ratio of $MgH_2/Mg(OH)_2$ for the characteristic peaks of MgH_2 at $2\theta = 27.9°$ and of $Mg(OH)_2$ at $2\theta = 18.5°$ for all of the investigated alloys (Table 2).

Because XRD analysis provides composition information to a maximum depth of 20 μm, we can compare the tendencies of the alloys to form $Mg(OH)_2$ on their surfaces. Based on data given in Table 2, there are thicker layers of hydroxide on the surface in the cases of the MgNi15 and MgNi34 alloys. In contrast, the MgNi26 and MgNi26Mm12 alloys exhibit some resistance to hydroxide formation. It can be assumed that the presence of large primary α-Mg or Mg_2Ni grains in the microstructure (Fig. 1a,c) promotes $Mg(OH)_2$ formation. In the opposite manner, fine eutectic structure and the presence of rare-earth metals (mischmetal) likely reduces hydroxide formation. Rare-earth metals exhibit electrochemical standard potentials that are similar to that of magnesium. Therefore, it seems reasonable to conclude that the addition of Mm reduces the driving force of galvanic corrosion, thus reducing the thickness of the magnesium-hydroxide surface layer.

3.3. Hydrogen evolution

The hydrogen evolution upon heating was monitored using the temperature-programmed desorption technique (TPD). The results from the TPD analyses of the hydrided alloys are shown in Fig. 3.

Because the XRD analysis detects only the magnesium hydride in these samples, we also subjected pure commercial MgH_2 powder to TPD analysis for comparison. The result of the TPD analysis of the pure MgH_2 powder is shown in Fig. 4.

From the hydrogen peaks of desorption that were obtained by the TPD analyses (Fig. 3), the temperatures of the start, maximum and end of the hydrogen evolution can be determined for each alloy. These temperatures, including the results for the pure MgH_2 powder, are given in Table 3.

The lowest temperature of the onset of hydrogen evolution is observed for the MgNi34 alloy (Fig. 3c). This observation might be attributed to the positive effect of nickel, which destabilises MgH_2 [25]. Therefore, nickel decreases the temperature of hydrogen desorption. However, this hypothesis fails in the cases of the MgNi15 and MgNi26 alloys. The MgNi26 alloy contains more nickel than the MgNi15 alloy, but the hydrogen evolution of this alloy (Fig. 3b) is observed at a higher temperature than that of the MgNi15 alloy (Fig. 3a). The onset-temperature difference between the MgNi15 and MgNi26 alloys is approximately 70 °C (Table 3). In this case, another factor than simple nickel content must play a significant role. Some papers indicate that the presence of $Mg(OH)_2$ or MgO

Table 3. Temperatures of the start, maximum and end of each hydrogen peak obtained by the TPD analyses of the hydrided alloys and pure MgH_2 powder

Sample	Temperature (℃)		
	Start of hydrogen peak	Maximum of hydrogen peak	End of hydrogen peak
MgNi15	148	211	298
MgNi26	216	278	318
MgNi34	125	230	297
MgNi26Mm12	183	257	349
MgH_2	376	414	463

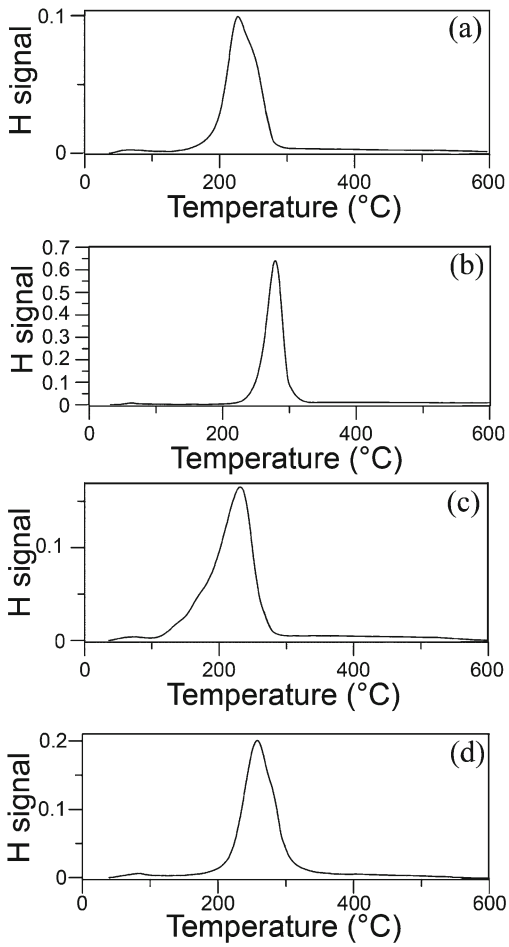

Fig. 3. The results of the TPD analysis of the hydrided (a) MgNi15, (b) MgNi26, (c) MgNi34 and (d) MgNi26Mm12 alloys.

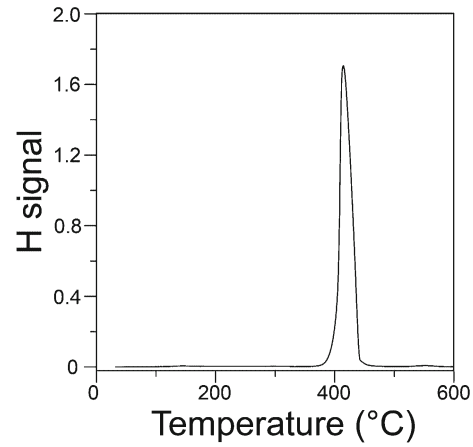

Fig. 4. The results of the TPD analysis of commercial MgH_2 powder.

on the surface of MgH_2 may serve as a catalyst for MgH_2 dissociation [30, 31], and as a result, the beginning of hydrogen evolution can be observed below 150 ℃. Indeed, in the cases of the MgNi15 and MgNi34 alloys, the H_2 evolution emerges at 148 and 125 ℃, respectively (Table 3). These two alloys exhibit high fractions of $Mg(OH)_2$ after electrochemical hydriding (Table 2), and therefore, a synergistic effect of Ni and $Mg(OH)_2$ most likely decreases the onset temperature of the decomposition of MgH_2 by more than 200 ℃ compared to pure MgH_2(Table 3). The temperature of hydrogen evolution for the MgNi26Mm12 alloy is not as low as that for MgNi34, but it is lower than that of the MgNi26 alloy by approximately 30 ℃. Most likely, large atoms of the rare-earth metals contained in the mischmetal deform the MgH_2 crystal lattice, thus weakening the Mg-H bonds and lowering the temperature of hydrogen evolution.

In terms of the MgH_2 destabilisation, we should also mention the fine eutectic mixture that is present in all of the investigated alloys (Fig. 1). The eutectic mixture contains a large number of interfaces, which may result in the formation of extra-fine magnesium hydride and in a reduction of its decomposition temperature compared to pure MgH_2. Indeed, structural refinement has been well known to reduce the decomposition temperatures of hydrides [18].

3.4. Hydrogen concentrations

The amount of absorbed hydrogen was obtained by integration of the hydrogen-peak area (Fig. 3). The total hydrogen concentrations achieved after the

Table 4. Hydrogen concentrations in the alloys after hydriding at 80 °C for 240 min

Alloy	MgNi15	MgNi26	MgNi34	MgNi26Mm12
Hydrogen concentration (wt.%)	0.65	1.24	1.02	1.06

electrochemical hydriding of the powdered alloys are summarised in Table 4. The maximum amount of absorbed hydrogen (approx. 1.3 wt.%) is observed for the MgNi26 alloy. The structure of the MgNi26 alloy is characterised by the fine eutectic mixture (Fig. 1b). The remaining binary alloys, namely, the MgNi15 and the MgNi34 alloys, achieved approximately 0.7 and 1.0 wt.% hydrogen, respectively. It seems that a higher fraction of eutectic present in the structure leads to the absorption of a greater amount of hydrogen. It was mentioned previously in this paper that a fine eutectic structure contains a large number of interfaces, which facilitate hydrogen diffusion. The large crystals of primary Mg and Mg_2Ni present in the MgNi15 and MgNi34 alloys, respectively, likely lowered the amount of absorbed hydrogen by forming thick layers of hydroxide (see Table 2). It is obvious that a layer of hydroxide on the surface significantly decreases the diffusion of hydrogen into the material. The MgNi26Mm12 alloy absorbed nearly the same amount of hydrogen as the MgNi34 alloy (see Table 4). However, taking into account the fact that the MgNi26Mm12 alloy contains a low quantity of the α-Mg phase that is suitable for MgH_2 formation, the ternary alloy seems to be more effective in terms of hydrogen absorption compared to the MgNi34 alloy. It can be assumed that the presence of Mm in the eutectic (Fig. 1d) promotes hydrogen absorption by stabilising the H atoms (together with nickel) [25] and by reducing magnesium-hydroxide formation (Table 2).

4. Conclusions

The dehydriding process of three Mg-Ni (hypoeutectic, eutectic, hypereutectic) alloys and one hypereutectic Mg-Ni-Mm alloy was studied via the TPD technique after electrochemical hydriding. The total amount of absorbed hydrogen was studied simultaneously. All samples of the hydrided alloys were in the powdered state. In the case of the Mg-Ni alloys, it was found that the amount of eutectic mixture in the structure directly influenced both the amount of absorbed hydrogen and the amount of magnesium hydroxide on the surface.

The highest content of hydrogen, nearly 1.3 wt.%, was achieved in the MgNi26 alloy, which can likely be attributed to its eutectic structure and its resistance to hydroxide formation. The hydrogen content achieved by the MgNi26 alloy is very similar to that of commercially used hydrides that are based on $LaNi_5$ or FeTi alloys. However, these alloys must be treated by long-term ball milling and high pressures of hydrogen before achieving their maximum hydrogen capacity of approximately 1.5 wt.% hydrogen [32]. In contrast, in this work, only moderate hydriding conditions with no prior ball milling were adopted.

The lowest temperature necessary for the beginning of MgH_2 decomposition was obtained for the MgNi34 alloy (125 °C). This temperature is lower than that of the decomposition of pure MgH_2 by approximately 250 °C. This significant reduction in temperature was most likely caused by the synergistic effect of nickel and magnesium hydroxide. The presence of mischmetal in the ternary MgNi26Mm12 alloy also decreased the temperature of MgH_2 decomposition compared to the MgNi26 alloy. However, mischmetal was not able to increase the amount of hydrogen absorbed during electrochemical hydriding.

Acknowledgement

The authors wish to thank the Czech Science Foundation (project no. P108/12/G043) for the financial support of this research.

References

[1] Ross, D. K.: Vacuum, *80*, 2006, p. 1084. doi:10.1016/j.vacuum.2006.03.030
[2] Wallace, W. E., Karlicek, R. F., Imamura, H.: J. Phys. Chem., *83*, 1979, p. 1708. doi:10.1021/j100476a006
[3] Huston, E. L., Sandrock, G. D.: J. Less-Common Met., *74*, 1980, p. 435. doi:10.1016/0022-5088(80)90182-4
[4] Aguey-Zinsou, K. F., Ares-Fernández, J. R.: Energy Environ. Sci., *3*, 2010, p. 526.
[5] Ouyang, L. Z., Yang, X. S., Dong, H. W., Zhu, M.: Scripta Mater., *61*, 2009, p. 339. doi:10.1016/j.scriptamat.2008.12.001
[6] Saita, I., Li, L., Saito, K., Akiyama, T.: J. Alloy. Compd., *356–357*, 2003, p. 490. doi:10.1016/S0925-8388(03)00230-5
[7] Denys, R. V., Zavaliy, I. Y., Paul-Boncour, V., Berezovets, V. V., Kovaľchuk, I. V., Riabov, A. B.: Intermetallics, *18*, 2010, p. 1579. doi:10.1016/j.intermet.2010.04.011
[8] Čermák, J., Král, L.: J. Hydrogen Energ., *33*, 2008, p. 7464. doi:10.1016/j.ijhydene.2008.09.042
[9] Vegge, T., Hedegaard-Jensen, L. S., Bonde, J., Munter, T. R., Nørskov, J. K.: J. Alloy. Compd., *386*, 2005, p. 1. doi:10.1016/j.jallcom.2004.03.143

[10] Song, Y., Guo, Z. X., Yang, R.: Mat. Sci. Eng. A-Struct., *365*, 2004, p. 73. doi:10.1016/j.msea.2003.09.008
[11] Mushnikov, N., Ermakov, A., Uimin, M., Gaviko, V., Terenťev, P., Skripov, A., Tankeev, A., Soloninin, A., Buzlukov, A.: Phys. Met. Metallogr., *102*, 2006, p. 421. doi:10.1134/S0031918X06100097
[12] Song, M.-Y., Hong, S.-H., Kwon, I.-H., Kwon, S.-N., Park, C.-G., Bae, J.-S.: J. Alloy. Compd., *398*, 2005, p. 283. doi:10.1016/j.jallcom.2005.02.014
[13] Jin, S.-A., Shim, J.-H., Cho, Y. W., Yi, K.-W.: J. Power Sources, *172*, 2007, p. 859. doi:10.1016/j.jpowsour.2007.04.090
[14] Imamura, H., Kusuhara, M., Minami, S., Matsumoto, M., Masanari, K., Sakata, Y., Itoh, K., Fukunaga, T.: Acta Mater., *51*, 2003, p. 6407. doi:10.1016/j.actamat.2003.08.010
[15] Huang, L.-J., Tang, J.-G., Wang, Y., Liu, J.-X., Wu, D. C.: J. Alloy. Compd., *485*, 2009, p. 186. doi:10.1016/j.jallcom.2009.05.131
[16] Yanghuan, Z., Dongliang, Z., Huiping, R., Shihai, G., Yan, Q., Xinlin, W.: Rare Metal Mat. Eng., *40*, 2011, p. 1146.
[17] Wu, Y., Han, W., Zhou, S. X., Lototsky, M. V., Solberg, J. K., Yartys, V. A.: J. Alloy. Compd., *466*, 2008, p. 176. doi:10.1016/j.jallcom.2007.11.128
[18] Niemann, M. U., Srinivasan, S. S., Phani, A. R., Kumar, A., Goswami, D. Y., Stefanakos, E. K.: J. Nanomater., *2008*, 2008, p. 1.
[19] Zhao, X., Ma, L.: J. Hydrogen Energ., *34*, 2009, p. 4788. doi:10.1016/j.ijhydene.2009.03.023
[20] Zhang, J., Villeroy, B., Knosp, B., Bernard, P., Latroche, M.: J. Hydrogen Energ., *37*, 2012, p. 5225. doi:10.1016/j.ijhydene.2011.12.096
[21] Mustafa, A.: J. Hydrogen Energ., *37*, 2012, p. 1905. doi:10.1016/j.ijhydene.2011.06.107
[22] Lee, S.-L., Hsu, F.-K., Chen, W.-C., Lin, C.-K., Lin, J.-C.: Intermetallics, *19*, 2011, p. 1953. doi:10.1016/j.intermet.2011.05.021
[23] Zhu, Y., Wang, Y., Li, L.: J. Hydrogen Energ., *33*, 2008, p. 2965. doi:10.1016/j.ijhydene.2008.04.003
[24] Huang, L. J., Liang, G. Y., Sun, Z. B.: J. Alloy. Compd., *421*, 2006, p. 279. doi:10.1016/j.jallcom.2005.11.039
[25] Vojtěch, D., Knotek, V.: J. Hydrogen Energ., *36*, 2011, p. 6689. doi:10.1016/j.ijhydene.2011.02.063
[26] Gale, W. F., Totemeier, T. C. (Eds.): Smithells Metals Reference Book. 8th ed. Amsterdam, Elsevier 2004.
[27] Løken, S., Solberg, J. K., Maehlen, J. P., Denys, R. V., Lototsky, M. V., Tarasov, B. P., Yartys, V. A.: J. Alloy. Compd., *446–447*, 2007, p. 114. doi:10.1016/j.jallcom.2006.11.200
[28] Denys, R. V., Riabov, A. B., Maehlen, J. P., Lototsky, M. V., Solberg, J. K., Yartys, V. A.: Acta Mater., *57*, 2009, p. 3989. doi:10.1016/j.actamat.2009.05.004
[29] Zhang, J., Zhou, D. W., He, L. P., Peng, P., Liu, J. S.: J. Phys. Chem. Solids, *70*, 2009, p. 32. doi:10.1016/j.jpcs.2008.09.018
[30] Leardini, F., Ares, J. R., Bodega, J., Fernández, J. F., Ferrer, I. J., Sánchez, C.: Phys. Chem. Chem. Phys., *12*, 2010, p. 572. doi:10.1039/b912964b
[31] Hammons, T. J.: J. Electric. Power Syst. Res., *28*, 2006, p. 548. doi:10.1016/j.ijepes.2006.04.001
[32] Sakintuna, B., Lamari-Darkrim, F., Hirscher, M.: J. Hydrogen Energ., *32*, 2007, p. 1121. doi:10.1016/j.ijhydene.2006.11.022